INTERNATIONAL JOURNAL OF HYDROGEN ENERGY 45 (2020) 18635–18644

Available online at www.sciencedirect.com

ScienceDirect

journal homepage: www.elsevier.com/locate/he

Development of RuO_2/CeO_2 heterostructure as an efficient OER electrocatalyst for alkaline water splitting

Sunil M. Galani, Aniruddha Mondal, Divesh N. Srivastava, Asit Baran Panda *

CSIR-Central Salt and Marine Chemicals Research Institute, Academy of Scientific and Innovative Research, CSIR-Human Research Development Centre (CSIR-HRDG) Campus, Sector-19, Kamla Nehru Nagar, Ghaziabad, 201002, India

HIGHLIGHTS

- Simple aqueous solution based Chemical Synthesis of RuO_2–CeO_2 hetero nanostructures.
- Synthesis is based on formation of CeO_2 spheres followed by Ru impregnation.
- 1 wt% RuO_2–CeO_2 showed excellent electrocatalytic OER activity in 1 M KOH solution.
- Showed low overpotential of 350 mV for 10 mA/cm^2 & Tafel slope of 74 mVdec^{-1} for OER.
- Exhibited superior electrochemical stability in basic as well as redox environment.

ARTICLE INFO

Article history:
Received 6 May 2019
Received in revised form
26 July 2019
Accepted 2 August 2019
Available online 14 September 2019

Keywords:
CeO_2
Ru
Nanostructure
Electrocatalyst
OER

ABSTRACT

Here, the synthesis of RuO_2 loaded CeO_2 with varying amount of Ru loading with enhanced amount of Ce^{3+} and surface area, through synthesis of CeO_2 using cerium ammonium carbonate complex as procure followed by Ru loading by impregnation and calcination at 300 °C, is presented. Corresponding characterizations by XRD, SEM, TEM, XPS of all the samples reveal the formation of highly crystalline mesoporous CeO_2 nanoparticles with uniformly dispersed RuO_2 particles on the CeO_2 surface having approximately 45% Ce^{3+}. All the samples were utilized as oxygen evolution reaction (OER) catalyst for electrocatalytic H_2 generation through water electrolysis. Electrocatalytic experiments reveal that synthesized 1 wt% RuO_2 loaded CeO_2 (1-RuO_2/CeO_2) showed superior OER activity. A quite low over-potential of 350 mV is required to attain a current density of 10 mA/cm^2 (η_{10}), with a Tafel slope of 74 mVdec^{-1} for OER in 1 M KOH solution. The synthesized 1-RuO_2/CeO_2 electrocatalyst also exhibited superior long term stability in basic medium and redox atmosphere.

Introduction

Development of sustainable and green energy source is one of the prime goal for the scientific community, to address faster growth of energy demand globally, limited stock of fossil fuels, and related extensive environmental pollution [1–3]. In this regards, hydrogen is supposed to be the more appropriate and perfect substitute to fossil fuel, owing to the superior specific

* *Corresponding author.*
E-mail address: abpanda@csmcri.res.in (A.B. Panda).
https://doi.org/10.1016/j.ijhydene.2019.08.026

energy density (143 MJ kg^{-1}), renewable, more importantly clean and generate only water on combustion [4–8]. Electrolysis of water into the oxygen and hydrogen is very well recognized route to generate hydrogen and played a significant role in the field of clean energy technologies [9–11]. In general, the dissociation of water molecules, commonly known as water splitting reaction, does take place into two half-reactions, specifically hydrogen evolution reaction (HER) and oxygen evolution reaction (OER) at cathode and anode, respectively [12–15]. However, due to the inherent sluggish kinetics both the reactions needs certain dynamic overpotential to overcome the energy barrier. In particular, overall H_2 generation efficiency is tremendously effected by high overpotential of OER as it is a multi-step 4 e-transfer process and need to drive the cell voltage around 1.8–2.0 V compared to the theoretical thermodynamic requirement of 1.23 V in electrocatalytic water splitting. Whereas HER required comparatively less overpotential [16,17]. Therefore, it is very essential to utilize outstanding electrocatalyst which can provide larger current density, low overpotential and also the excellent stability [18–20]. Over the last few decades, enormous efforts has been made to find practically useful, efficient anode materials, i.e., OER catalyst [21–48].

Among the reported OER catalysts, ruthenium oxide (RuO_2) is the most effective electrocatalysts owing to its enhanced electrical conductivity, reversible redox property, wide potential window and more importantly low overpotential [30–48]. However, ruthenium is not abundant and costly, which hinders its extensive utilization in large-scale. Thus, reduction of catalyst loading without compromising the overall efficiency is one of the most appropriate strategy and which can be achieved by reduction of size in nanometer level to enhance specific surface area. Unfortunately, OER activity of RuO_2 nanoparticles (NP) are highly affected by its inferior cycling stability, due to the particle growth during cycling and oxidation of Ru to higher oxidation state [32–36]. Many studies have shown that Ru with oxidation state of IV is the more efficient for H_2O splitting [30,31]. Still, it is one of the most important strategy to develop highly active stable nanostructured Ru based cost-effective electrocatalyst to conduct large scale OER in low overpotential [37–48]. In this direction, supported RuO_2 is most appealing alternative, where support not only stabilize the RuO_2 NP and restrict agglomeration, but also prevent over-oxidation [31,40,44–48]. In this regards, support with redox property is the most appropriate and investigation of suitable support with high surface area is very essential.

Ceria (CeO_2) is a technologically most important abundant rare-earth oxide [49–54]. It is widely used in different redox reaction due to its reasonable reversible oxygen storage ability for its characteristic Ce^{3+}/Ce^{4+} red-ox properties. Consequently, different cerium supported Ru (Ru–CeO_2) based catalysts has also been developed and used as effective catalyst for large variety of redox reactions [49,55–58]. However, use of Ru–CeO_2 based catalyst for water electrolysis is very rare [47,48]. Zhu and his group [47] and Demir et al. [48] studied OER activity of RuO_2/CeO_2 and Ru (nanoparticle)-CeO_2, respectively. The reported OER activity of both the catalysts are quite good, but the activity is far behind to that of the state of the art catalyst pure RuO_2. However, there is a huge opportunity to improve the activity. It is well established that, the catalytic activity of CeO_2 based catalysts ate highly dependent on the degree of defect i.e., Ce^{3+}/Ce^{4+} ratio, particle size, morphology, and surface area, which are highly controlled by the precursor and synthetic procedure [49–54]. To improve Ce^{3+}/Ce^{4+} Zhu and his group [47] used Ag–CeO_2 based method which is complicated and not cost effective. Recently, we have established that aqueous metal ammonium carbonate complex solutions are novel precursors for the synthesis of high quality nanostructured materials [59–61]. Respective cerium ammonium carbonate complex solutions is also a unique precursor for the synthesized CeO_2 with high surface area with high surface defect [50,52–54].

In the direction to develop cost effective and efficient RuO_2–CeO_2 based OER catalyst, herein we report the development of RuO_2 loaded CeO_2 (RuO_2/CeO_2) with varying RuO_2 loading as efficient and stable electrocatalyst for OER. Aqueous cerium ammonium carbonate complex solution was utilized for the synthesis of bare CeO_2 and RuO_2 was loaded by impregnation method. The synthesized RuO_2/CeO_2 contain uniformly dispersed RuO_2 nanoparticles on highly crystalline CeO_2 with high surface area and enhanced surface defect. Particularly 1% RuO_2 loaded catalyst showed superior OER activity in basic medium.

Experimental section

Chemicals

Analytical grade Ceric ammonium nitrate [$(NH_4)_2Ce(NO_3)_6$], sodium hydroxide, ammonium carbonate and acetone extra pure (CH_3COCH_3) were procured from s. d. fine Chemical, India. Ruthenium(III) chloride was procured from sigma Aldrich. The experiments were made using water with 18 MΩ cm.

Synthesis of CeO_2 nanoparticles

Aqueous ammonium carbonate complex solution, prepared using our previously developed, was utilized as precursor for the synthesis of bare CeO_2 nanoparticles and any additional stabelizing or structure directing agent was not employed during synthesis [52–54]. In a typical synthetic procedure, to a 100 ml saturated ammonium carbonate solution 100 mL aqueous solution of ceric ammonium nitrate [$(NH_4)_2Ce(NO_3)_6$] (15 g) was added dropwise with constant stirring (500 rpm) and stirring was continued for another 10 min. Solid ammonium carbonate was added to the precursor solution to maintain the pH of the solution to 9 during the stirring period. White precipitate was formed immediate after the addition of Ce solution which was re-dissolved on stirring and finally resulted a clear solution. Then the obtained clear precursor solution mixture was hydrothermally treated at 150 °C for 6 h using a Teflon lined stainless steel autoclave. The resultant precipitate obtained after cooling the autoclave was washed properly by deionized water and dried at 70 °C for overnight. Lastly, the calcination of the dried powder was performed at 300 °C for 3 h.

Synthesis of RuO_2/CeO_2

RuO_2/CeO_2 was synthesized through the impregnation method. For optimization amount of Ru was varied and used 1, 2.5, 5 and 10 wt % Ru with respect to that of CeO_2. In a typical synthetic procedure, the 1 g of the CeO_2 sample obtained after hydrothermal treatment followed by drying was dispersed well in ml deionized water, to the suspension freshly prepared 30 ml Ruthenium(III) chloride solution, containing required amount of Ru, added drop wide and finally the pH of the solution was adjusted to 13 by adding the 12N NaOH solution and stirring for 24 h at room temperature. Finally the resultant material was collected, washed thoroughly and dried overnight at 70 °C. The dried powder was calcined at 300 °C for 6 h. Here after, the synthesized RuO_2/CeO_2 with varying amount of Ru will be termed as "x-RuO_2/CeO_2" where x is wt% of Ru. As for example the RuO_2/CeO_2 catalyst with 1 wt% Ru will be termed as 1-RuO_2/CeO_2.

Characterization

X-ray diffraction patterns of the synthesized samples were recorded using Rigaku Miniflex X-ray powder diffractometer. Electron microscopic images of the synthesized catalysts were collected by JEOL JSM 7100F Field Emission Scanning Electron Microscope (FE-SEM) were used and JEOL JEM 2100 Transmission Electronic Microscope (TEM). ESCALAB 250 XPS System was utilized to record the X-ray photoelectron spectroscopy (XPS).

Electrochemical performances

The electrochemical HER activity of the synthesized sample was evaluated using Metrohm Autolab PGSTAT204 potentiostat/galvanostat electrochemical workstation. For the measurementa a glassy carbon electrode (GCE) of mm in diameter or synthesized material modified correspponding GCE as the working electrode, Graphite as counter electrode and Ag/AgCl (sat. KCl) as the reference electrode, was wtilized. Before measurement, the bare GCE was mirror polished, using alumina powder (0.3 μm) and nylon pad, follo by washing through sonication for 30 min using 1:1 acetone-water mixture and dried properly. Seperately, 5 mg of catalyst was properly suspended in 1 mL solution mixture having 100 μL Nafion solutions (0.5 wt%) and 900 μL of DMF by ultrasonication for 45 min. After proper dispersion, 10 μL dispersed catalyst ink was loaded on cleaned and dried GCE through drop casting and dried under ambient atmospherec condition for overnight (loading 0.28 mg cm^{-2}). As electrolyte 1 M KOH solution was used. Linear sweep voltammetry (LSV) at 5 mV/s scan rate and in the range of +0.3 V to +2.0 V was performed. EIS at a frequency range of 10 mHz–300 mHz in a fixed DC potential of −0.4 V vs R.H.E was also performed. The chronoamperometry experiment for 12 h at an over potential of 0.3 V (in 1M KOH) was done to verify the long term stability. The detailed sample preparation techniques have also been discussed in see our previously published articles [8,11].

Results and discussion

XRD patterns of all the synthesized bare CeO_2 as well as RuO_2/CeO_2 nanoparticles with varying RuO_2 loading exhibited identical well-resolved x-ray diffraction patterns (Fig. 1a–d). The peaks at 2θ = 28.5, 33.0, 47.4, 56.3, 59.4, 70.0 and 76.8 ascribed to the (111), (200), (220), (311), (222), (400), and (331) planes of cubic fluorite structure of CeO_2 (JCPDS 34-0394), respectively, with a space group of Fm^{-3} m. In the XRD pattern of 1-RuO_2/CeO_2 and 2.5-RuO_2/CeO_2 any distinguishable diffraction peak for either metallic ruthenium or ruthenium oxide was not identified. However in the XRD pattern of 5-RuO_2/CeO_2 and 10-RuO_2/CeO_2 three low intense peaks at 25.5, 35.1 and 54.4 recognize to the (110), (101) and (211) planes of RuO_2 (JCPDS 88-0322), respectively, was observed, in addition to that of characteristic peaks for CeO_2. Till 2.5% RuO_2 loaded CeO_2 respective diffraction peak for RuO_2 was not observed most probably due to the presence of lower amount homogeneously distributed RuO_2 in CeO_2 moiety, which is beyond the identification level of XRD instrument. The crystallite size of all the synthesized CeO_2 are almost same, which is more or less 6 nm, and crystallite sizes were calculated from the line broadening of respective XRD pattern using Scherrer formula.

Morphology of the synthesized bare CeO_2 and RuO_2/CeO_2 nanostructured materials were investigated by FESEM analysis. Low-magnified SEM image of bare CeO_2 indicate that the presence of mostly spheres in the size range of 500 nm to 2 μm (Fig. 2a). The corresponding magnified images showed the smooth surface of the synthesized spheres (Fig. 2b). In addition to that of spherical morphology some aggregated particles was also identified. However, in the RuO_2/CeO_2 materials such individual spheres with smooth surface was rarely identified (Fig. 2c) and mostly aggregated spherical morphology was observed. Most probably during the

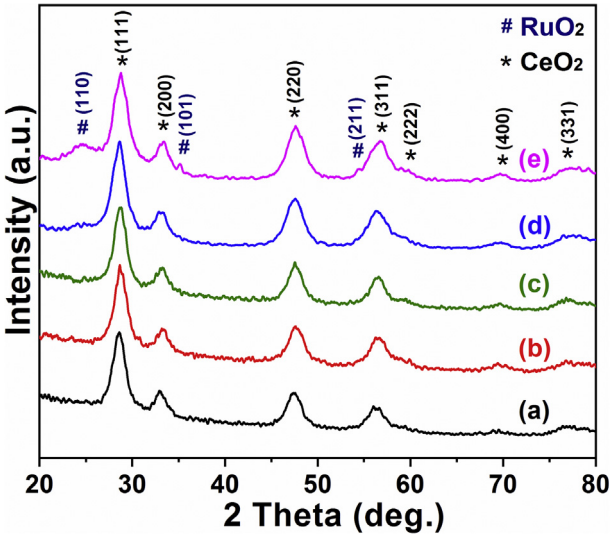

Fig. 1 – XRD pattern of synthesized (a) bare CeO_2, (b) 1-RuO_2/CeO_2, (c) 2.5-RuO_2/CeO_2, (d) 5-RuO_2/CeO_2 and (e) 10-RuO_2/CeO_2 nanostructured materials calcined at 300 °C/6 h.

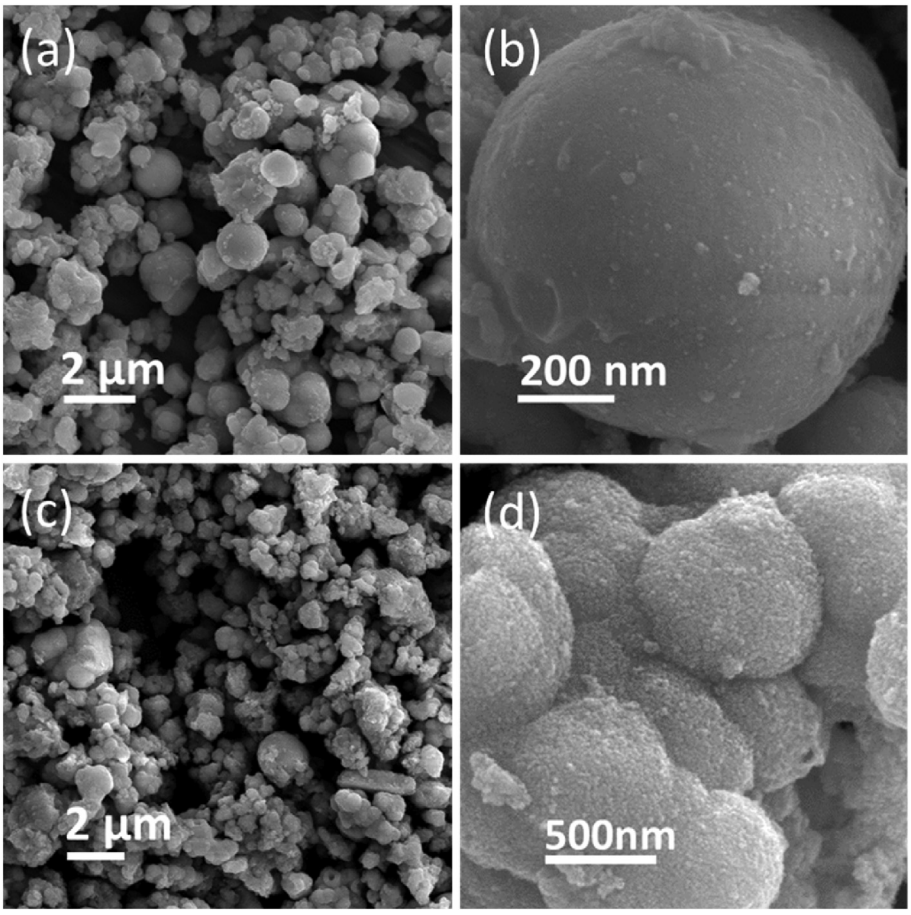

Fig. 2 – FESEM images of synthesized bare CeO_2 (a, b), and 1-RuO_2/CeO_2 (c, d) nanostructured materials calcined at 300 °C/ 6 h.

impregnation process the individual spheres were damaged. Corresponding magnified images evidenced the presence of mostly aggregated spheres. The surface of the spheres are rough and individual spheres were formed by the aggregation of very small particles (Fig. 2d).

Further detailed morphological and microstructural study of the synthesized samples were made using transmission electron microscopy (TEM) (Fig. 3). Low magnified TEM image of bare CeO_2 further evidenced the formation spherical structure (Fig. 3a). The individual spheres are porous and composed by nanoparticles in the size range of 5–8 nm (Fig. 3b–c). Corresponding HR-TEM image of the bare CeO_2 demonstrated the presence of distinct lattice fringe with an inter-planer distance of 0.32 nm, corresponding to the (111) plane of CeO_2, further confirm the formation of highly crystalline CeO_2 nanoparticles (Fig. 3d). The magnified image of 1-RuO_2/CeO_2 sample indicate the presence of very small (~1 nm) particles on the surface of the particles with comparatively higher sized (Fig. 3e). The image also showed the presence of pores in the range of 3–5 nm. Corresponding HR-TEM images showed the presence of distinct lattice fringes in bigger particles with the inter-planer distance is 0.32 nm similar to that of bare CeO_2. Unfortunately, we were unable to focus the smaller particles, marked by white circles, to get the fringes (Fig. 3f). However, it can be presumed that the smaller particles are the RuO_2 particles uniformly dispersed on the surface of the CeO_2 particles.

Fig. 4 represents the X-ray photoemission spectra (XPS) of 1-RuO_2/CeO_2 nanospheres. The XPS survey spectrum clearly evidenced the presence of ruthenium (Ru), cerium (Ce) and oxygen (O) (Fig. 4a). Corresponding, deconvoluted O1s core level spectrum (Fig. 4b) showed the presence of three peaks at around 529.4 eV, 530.9 eV and 532.7 eV, which can be ascribed to the lattice oxygen coordinated to Ce^{4+}, the surface oxygen species assigned to defect oxide sites i.e., coordinated to Ce^{3+}, and surface hydroxyl group, respectively [48,51]. The Ru 3d XPS spectra (Fig. 4c) of the catalysts show a doublet peaks around 281.1 eV and 286.5 eV attributed to $Ru^{IV}O_2$ oxidation state. The deconvoluted core level spectra in the range of 875–925 eV, showed the presence of fitted 2 sets of spin-orbit split doublets of Ce 3d ($3d_{5/2}$ and $3d_{3/2}$) and endorse the coexistence of both Ce^{3+} and Ce^{4+} (Fig. 4d) [48,51]. The characteristic peaks at 880.7, 885.5, 899.1 and 903.6 eV belong to Ce^{3+}. The other set of peaks at 882.7, 888.6, 898.9, 901.2, 907.0 and 917.0 eV are related to Ce^{4+}. Corresponding area calculation reveal the presence of 46.7% Ce^{3+} (Ce^{3+}/Ce T%) and 53.3% Ce^{4+} (Ce^{4+}/Ce T%) in the synthesized 1-RuO_2/CeO_2 nanospheres (Table S1, Supporting Information).

Fig. 5 represents the nitrogen adsorption-desorption isotherm and corresponding pore size distribution of the

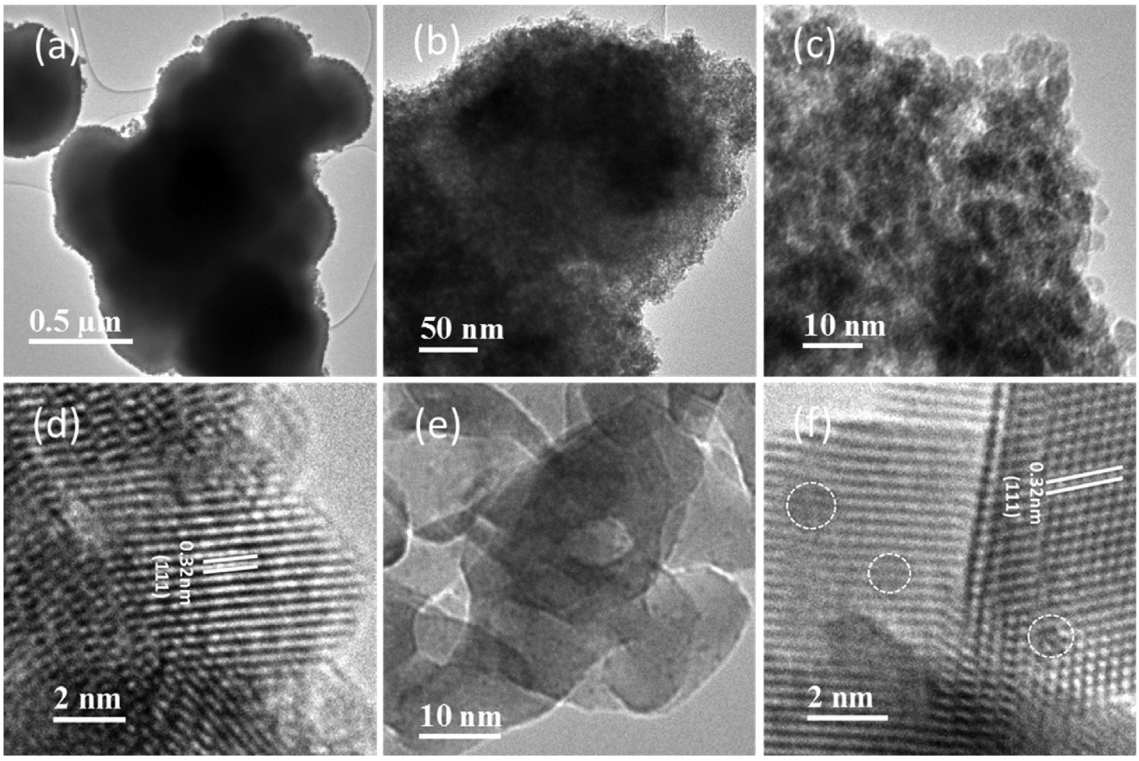

Fig. 3 – TEM and HR-TEM images of synthesized bare CeO_2 (a–d) and 1-RuO_2/CeO_2 (e–f) nanostructured materials calcined at 300 °C/6 h.

synthesized bare CeO_2 and 1-RuO_2/CeO_2 nanospheres and both the sample showed almost identical sorption pattern. Both the isotherm correspond to the type IV, having a hysteresis loop of H3 type (according to the IUPAC classification), and reveal the formation for mesoporous materials. Other Ru loaded CeO_2, i.e., 2.5-RuO_2/CeO_2, 5-RuO_2/CeO_2 and 10-RuO_2/CeO_2, also showed similar sorption isotherm (Fig. S1). The total BET surface area of the synthesized pure CeO_2 is 103 m^2/g. However, surprisingly the surface area of Ru-loaded CeO_2 samples are quite high, which is in the range of 148–166 m^2/g, instead to expected reduction of surface area due to pore blockage by Ru nanoparticles (Table S2). This is most probably due to the breaking of bare CeO_2 spheres with smooth surface and formation of small particle assembled spheres during impregnation of Ru. All the samples showed very narrow pore size distribution, calculated using BJH method from the desorption part of the sorption isotherm, with are in the range of 3–6 nm.

Electrocatalytic OER performance

All the as synthesized materials, such as bare CeO_2, 1-RuO_2/CeO_2, 2.5-RuO_2/CeO_2, 5-RuO_2/CeO_2 was used for the evaluation of electrocatalytic Oxygen Evolution Reaction (OER) performance at room temperature. Due to that, the above mentioned materials was loaded on the surface of glassy carbon electrode (GCE). The OER test was performed in a nitrogen (N_2) gas saturated 1M KOH solution with the three electrode system. The iR corrected linear seep voltammetry (LSV) was done at 5 mV/s scan rate in three electrode set up to minimize the capacitive currents. The anodic polarization curves of the synthesized materials was shown in Fig. 6a. All the synthesized bare and RuO_2 loaded CeO_2 samples showed more or less OER activity. However, 1-RuO_2/CeO_2 showed superior electrocatalytic OER activity with a quite lower onset over potential. The estimation of the necessary overpotential to reach a 10 mA/cm^2 current density (η_{10}) is supposed to be the vital parameter for OER, as it resemble with the 10% effective solar water-splitting [27], and corresponding η_{10} of the synthesized samples are marked by dotted lines in the respective LSV curve. The respective η_{10}, i.e., required overpotential to realize the current density of 10 mA/cm^2, for 1-RuO_2/CeO_2 is 350 mV for OER. However, the η_{10} for other samples are comperatively quite high, which are 580 mV, 460 mV and 510 mV for bare CeO_2, 2.5-RuO_2/CeO_2, 5-RuO_2/CeO_2, respectively.

To determine the steady state of the electrocatalytic reaction, Tafel slope was calculatted from the corresponding LSV curves of the synthesized materials. In general, lower Tafel slope resembles the enhanced catalytic activity [62]. Fig. 6b represents the corresponding Tafel slope of the synthesized samples. The lower Tafel slope of 74 mVdec^{-1} towards OER activity of 1-RuO_2/CeO_2, compared to that of bare CeO_2, 2.5-RuO_2/CeO_2 and 5-RuO_2/CeO_2 with Tafel slopes of 131, 89 and 93 mVdec^{-1}, respectively, further supports the superior electrocatalytic OER activity of 1-RuO_2/CeO_2. The enhanced electrocatalytic activity of the 1-RuO_2/CeO_2 catalyst is most probably due to the mesoporous structure with homogeneously distributed RuO_2 particles and enhanced surface area. The porous structure facilitate easy penetration of electrolytes to respective active sites of the synthesized materials. Additionally, the formation of heterostructure of RuO_2 and CeO_2

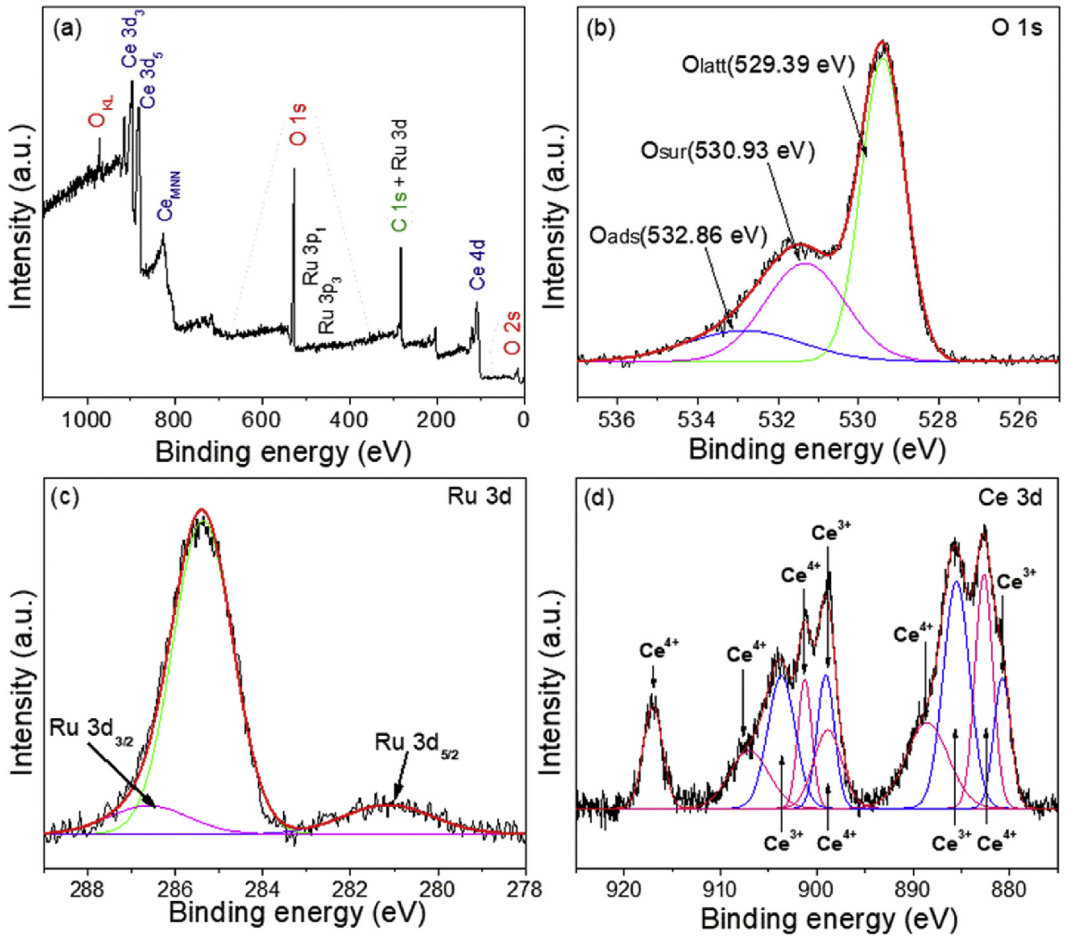

Fig. 4 – XPS survey spectrum (a), high resolution O 1s (b), Ru 3d (c), and Ce 3d (d) spectra of synthesized 1-RuO_2/CeO_2 nanostructured material calcined at 300 °C/6 h.

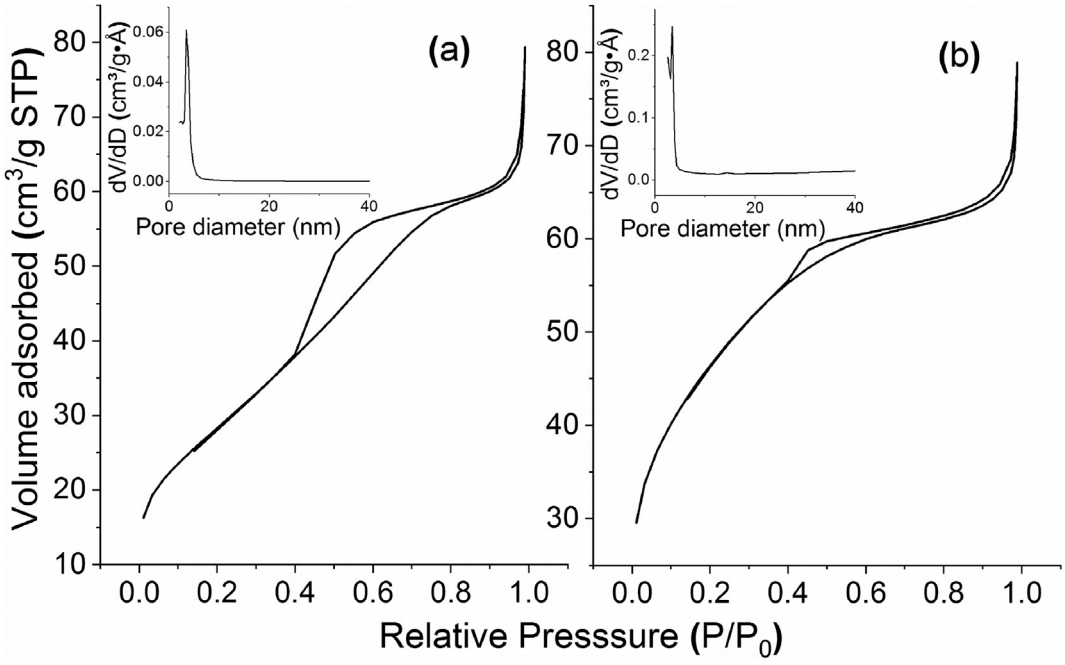

Fig. 5 – The nitrogen sorption isotherm and corresponding pore size distribution curve (inset) of synthesized bare CeO_2 (a) and 1- RuO_2/CeO_2 (b) nanostructured materials calcination at 300 °C for 6 h.

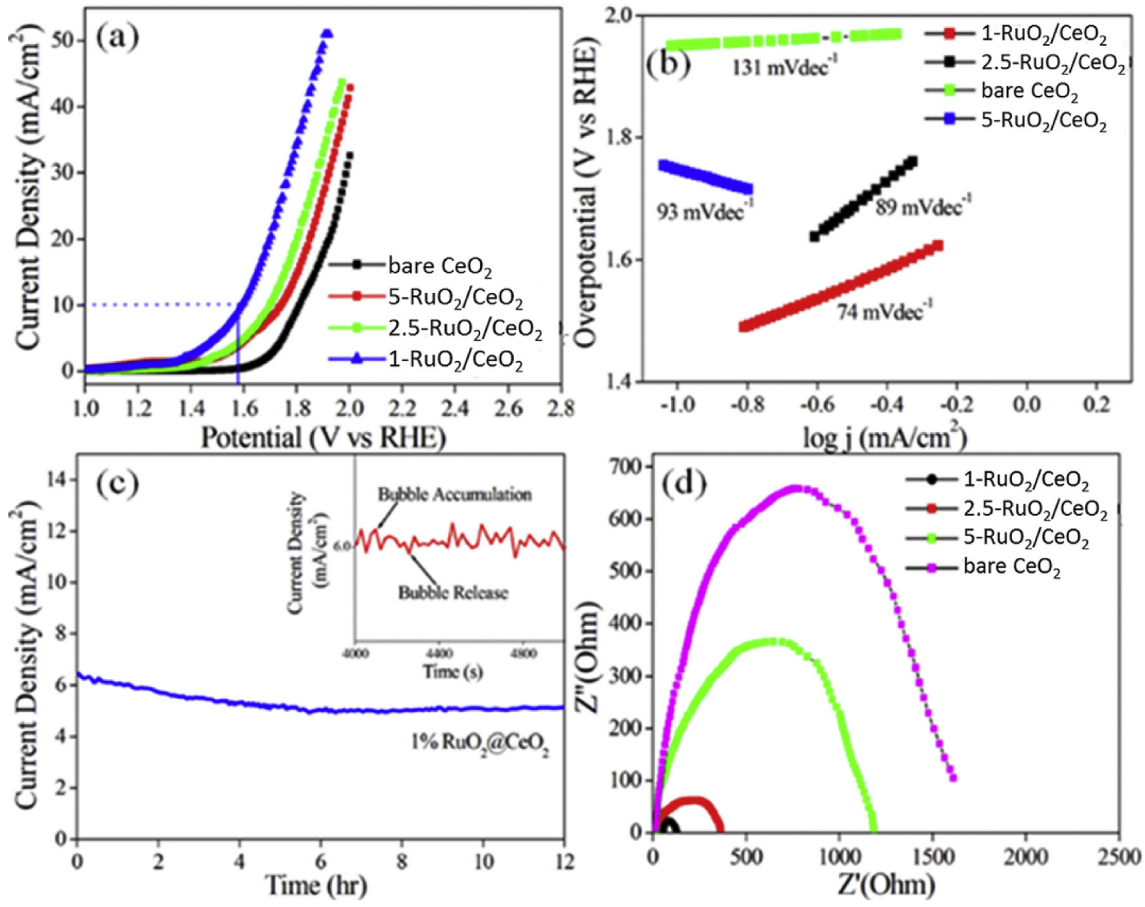

Fig. 6 – (a) Linear sweep voltammetry curves with iR correction and corresponding Tafel plot (b) of synthesized bare CeO_2, 1-RuO_2/CeO_2, 2.5- RuO_2/CeO_2, 5- RuO_2/CeO_2 modified GCE in 1M KOH at a scan rate of 5 mV/S for OER, (c) chronoamperometric experiment of 1- RuO_2/CeO_2 at a constant polarization potential of 1.60 V (Vs RHE) in N_2 saturated 1M KOH solution at room temperature and the inset shows the corresponding current densities at the time between ~66 and 83min, and (d) the impedance spectroscopy of all the samples.

was also facilitate the electrocatalysis process. Furthermore, the increased amount of RuO_2 on the surface of CeO_2 had blocked the active site for the further electrocatalytic reactions.

The long term stability of the synthesized catalysts was examined by chronoamperometry in a 1 M KOH solution. Chronoamperometry experiment of the optimized electrocatalyst 1-RuO_2/CeO_2 was performed by applying 1.6 V (Vs RHE) potentiostatically for 12 h. The current density was monitor during the 12 h experiment and the corresponding result is shown in Fig. 6c. Due to constant and steady generation and liberation of formed bubble, it resulted stable Zig-Zag output and evidenced the synthesized material is stable enough in basic solution (1 M KOH).

Furthermore, electrochemical impedance spectroscopy (EIS) was performed to evaluate the charge transfer resistance (R_{ct}) of the synthesized materials for verification of the respective OER kinetics. Fig. 6d shows the respective Nyquist plot of the synthesized materials. From the respective Nyquist plot data, it was clearly indicate the 1-RuO_2/CeO_2 possesses the minimum curvature and signifies the low charge transfer resistance among all synthesized samples. This is most probably due to the formation of optimised heterojunction of 1-RuO_2/CeO_2 than other samples which shows low R_{ct} values and helped to pass the charge easily.

For the further verification of the stability in red-ox environment, we performed the cyclic voltammetry (CV) for 2000 cycle and performed the LSV before and after in 1M KOH at 5 mV/s of 1% RuO_2/CeO_2. To check the stability, LSV of fresh 1-RuO_2/CeO_2 catalyst loaded GCE was taken, and then CV was performed for 2000 cycle and further LSV of this catalyst was taken. The corresponding result was shown in Fig. S2. After the complete cyclic voltammetry test, almost indistinguishable polarization curve (98%) proved the excellent redox stability of the 1% RuO_2/CeO_2.

Electrochemical active surface area (EASA) of an electrocatalyst is a crucial factor for corresponding OER activity and it very essential to evaluate to assess the origin the overall electrocatalytic activity. EASA is highly related to that of electrochemical double layer capacitance and EASA is directly proportional to capacitance. To evaluate EASA, CV of all the synthesized catalyst was achieved in 1 M KOH solution at a scan rate range of 5–200 mV/s and the potential range of 1.50 V–1.60 V, to enumerate their double layer capacitance. The respective CV and corresponding plot of scan rate Vs.

current density is presented in Fig. S3. The synthesized 1% RuO_2/CeO_2 showed maximum double layer capacitance of 23000 μF/cm^2 with respect to that of other synthesized samples (Table S3). The respective EASA was calculated using the equation;

$$A_{ECSA} = \frac{Capacitance\ Double\ layer(Cdl)}{40\ \mu F/cm^2(Cs)} per\ cm^2$$

As expected, the 1% RuO_2/CeO_2 showed maximum EASA of 575 cm^2 to that of other samples (Table S3). EASA result also further support the superior catalytic activity of 1- RuO_2/CeO_2.

The enhanced electrocatalytic activity of the 1-RuO_2/CeO_2 catalyst is most probably due to the mesoporous structure with homogeneously distributed RuO_2 nanoparticles, enhanced degree of defect in crystalline support CeO_2, i.e., Ce^{3+}/Ce^{4+} ratio, and enhanced surface area. The porous structure facilitate easy penetration of electrolytes to respective active sites of the synthesized materials and resulted the superior EASA. Additionally, the formation of heterostructure of RuO_2 and CeO_2 was also facilitate the electrocatalysis process. In the RuO_2/CeO_2 with higher Ru loading, active site reduction took place not only for particle growth but also for blockage of pores.

Conclusion

In summary, we have developed a facile synthetic protocol for mesoporous and crystalline RuO_2 loaded CeO_2 nanostructures. The synthesized 1- RuO_2/CeO_2 showed enhanced electrocatalytic behavior towards the OER with good kinetics in 1 M KOH solution and current of 10 mA/cm^{-2} was achieved at quite low overpotential of 350 mV with 74 mV dec^{-1} Tafel slope which is also quite low. Due to the presence of mesoporosity, optimized superior heterojunction between RuO_2 and CeO_2 facilitates the accumulation of more electrolyte and consequent electron transportation. The synthesized materials also showed excellent stability in basic medium. Thus, the superior OER activity with long-term stability make the synthesized 1-RuO_2/CeO_2 nanostructured material as a promising OER catalyst for O_2 generation through electrolysis of water in large scale.

Funding

This work was supported by Science and Engineering Research Board (SERB), Department of Science and Technology, Government of India [Grant numbers EMR/2014/001219].

Acknowledgements

CSIR-CSMCRI Communication No. 098/2019. Authors would like to acknowledge SERB, India (EMR/2014/001219) for financial support. Aniruddha Mondal, acknowledges ONGC India, for fellowship. The authors acknowledge the "AESDCIF" of CSMCRI for providing instrumentation facilities.

Appendix A. Supplementary data

Supplementary data to this article can be found online at https://doi.org/10.1016/j.ijhydene.2019.08.026.

REFERENCES

[1] Omer AM. Energy, environment and sustainable development. Renew Sustain Energy Rev 2008;12:2265–300. https://doi.org/10.1016/j.rser.2007.05.001.
[2] Acar C, Dincer I. Comparative assessment of hydrogen production methods from renewable and non-renewable sources. Int J Hydrogen Energy 2014;39:1–12. https://doi.org/10.1016/j.ijhydene.2013.10.060.
[3] Dunn S. Hydrogen futures: toward a sustainable energy System. Int J Hydrogen Energy 2002;27:235–64. https://doi.org/10.1016/S0360-3199(01)00131-8.
[4] Winter CJ. Hydrogen energy -abundant, efficient, clean: a debate over the energy-system-of-change. Int J Hydrogen Energy 2009;34:S1–52. https://doi.org/10.1016/j.ijhydene.2009.05.063.
[5] Holladay JD, Hu J, King DL, Wang Y. An overview of hydrogen production technologies. Catal Today 2009;139:244–60. https://doi.org/10.1016/j.cattod.2008.08.039.
[6] Saha A, Sinhamahapatra A, Kang TH, Ghosh SC, Yu JS, Panda AB. Hydrogenated MoS_2 QD-TiO_2 heterojunction mediated efficient solar hydrogen production. Nanoscale 2017;9:17029–36. https://doi.org/10.1039/C7NR06526D.
[7] Liu J, Liu Y, Liu NY, Han YZ, Zhang X, Huang H, et al. Metal-free efficient photocatalyst for stable visible water splitting via a two-electron pathway. Science 2015;347:970–4. https://doi.org/10.1126/science.aaa3145.
[8] Saha A, Paul A, Srivastava DN, Panda AB. Porous carbon incorporated β-Mo2C hollow sphere: an efficient electrocatalyst for hydrogen evolution reaction. Int J Hydrogen Energy 2018;43:21655–64. https://doi.org/10.1016/j.ijhydene.2018.04.051.
[9] Jiao Y, Zheng Y, Jaroniec M, Qiao SZ. Design of electrocatalysts for oxygen- and hydrogen-involving energy conversion reactions. Chem Soc Rev 2015;44:2060–86. https://doi.org/10.1039/C4CS00470A.
[10] Carmo M, Fritz DL, Mergel J, Stolten DA. Comprehensive review on PEM water electrolysis. Int J Hydrogen Energy 2013;38:4901–34. https://doi.org/10.1016/j.ijhydene.2013.01.151.
[11] Mondal A, Paul A, Srivastava DN, Panda AB. Defect- and phase-induced acceleration of electrocatalytic hydrogen production by ultrathin and small MoS2-decorated rGO sheets. ACS Appl Nano Mater 2018;1:4622–32. https://doi.org/10.1021/acsanm.8b00914.
[12] Wei C, Rao RR, Peng J, Huang B, Stephens IEL, Risch M, et al. Recommended practices and benchmark activity for hydrogen and oxygen electrocatalysis in water splitting and fuel cells. Adv Mater 2019:1806296. https://doi.org/10.1002/adma.201806296.
[13] Seo B, Sa YJ, Woo J, Kwon K, Park J, Shin TJ, et al. Size-dependent activity trends combined with in situ X-ray absorption spectroscopy reveal insights into cobalt oxide/carbon nanotube-catalyzed bifunctional oxygen electrocatalysis. ACS Catal 2016;6:4347–55. https://doi.org/10.1021/acscatal.6b00553.
[14] Shao D, Li P, Zhang R, Zhao C, Wang D, Zhao C. One-step preparation of Fe-doped Ni_3S_2/rGO@NF electrode and its superior OER performances. Int J Hydrogen Energy 2019;44:2664–74. https://doi:10.1016/j.ijhydene.2018.11.054.

[15] Ding J, Ji S, Wang H, Gai H, Liu F, Linkov V, et al. Mesoporous nickel-sulfide/nickel/N-doped carbon as HER and OER bifunctional electrocatalyst for water electrolysis. Int J Hydrogen Energy 2019;44:2832–40. https://doi.org/10.1016/j.ijhydene.2018.12.031.
[16] Xu Z, Pan H, Lin Y, Yang Z, Wang J, Gong Y. Constructing a hexagonal copper-coin-shaped $NiCoSe_2$@NiO@$CoNi_2S_4$ @CoS_2 hybrid nanoarray on nickel foam as a robust oxygen evolution reaction electrocatalyst. J Mater Chem 2018;6:18641–8. https://doi.org/10.1039/C8TA06084C.
[17] Zhu W, Yue Z, Zhang W, Hu N, Luo Z, Ren M, et al. Wet-chemistry topotactic synthesis of bimetallic iron–nickel sulfide nanoarrays: an advanced and versatile catalyst for energy efficient overall water and urea electrolysis. J Mater Chem 2018;6:4346–53. https://doi.org/10.1039/C7TA10584C.
[18] Bartels JR, Pate MB, Olson NK. An economic survey of hydrogen production from conventional and alternative energy sources. Int J Hydrogen Energy 2010;35:8371–84. https://doi.org/10.1016/j.ijhydene.2010.04.035.
[19] Zeng K, Zhang D. Recent progress in alkaline water electrolysis for hydrogen production and applications. Prog Energy Combust Sci 2010;36:307–26. https://doi.org/10.1016/j.pecs.2009.11.002.
[20] Sun H, Yan Z, Liu F, Xu W, Cheng F, Chen J. Self-supported transition-metal-based electrocatalysts for hydrogen and oxygen evolution. Adv Mater 2019. https://doi.org/10.1002/adma.201806326. 1806326.
[21] Weng B, Wang X, Grice CR, Xu F, Yan Y. A new metal–organic open framework enabling facile synthesis of carbon encapsulated transition metal phosphide/sulfide nanoparticle electrocatalysts. J Mater Chem 2019;7:7168–78. https://doi.org/10.1039/C9TA00404A.
[22] Jiao L, Zhou YX, Jiang HL. Metal-Organic framework-based CoP/reduced graphene oxide: high- performance bifunctional electrocatalyst for overall water splitting. Chem Sci 2016;7:1690–5. https://doi.org/10.1039/C5SC04425A.
[23] Suen NT, Hung SF, Quan Q, Zhang N, Xu YJ, Chen HM. Electrocatalysis for the oxygen evolution reaction: recent development and future perspectives. Chem Soc Rev 2017;46:337–65. https://doi.org/10.1039/C6CS00328A.
[24] Dinh KN, Liang Q, Du C-F, Zhao J, Tok AIY, Mao H, et al. Nanostructured metallic transition metal carbides, nitrides, phosphides, and borides for energy storage and conversion. Nano Today 2019;25:99–121. https://doi.org/10.1016/j.nantod.2019.02.008.
[25] Guo Y, Park T, Yi JW, Henzie J, Kim J, Wang Z, et al. Nanoarchitectonics for transition-metal-sulfide-based electrocatalysts for water splitting. Adv Mater 2019. https://doi.org/10.1002/adma.201807134. 1807134.
[26] Ali Y, Nguyen VT, Nguyen NA, Shin S, Choi HS. Transition-metal-based NiCoS/C-dot nanoflower as a stable electrocatalyst for hydrogen evolution reaction. Int J Hydrogen Energy 2019;44:8214–22. https://doi.org/10.1016/j.ijhydene.2019.01.297.
[27] Mondal A, Paul A, Srivastava DN, Panda AB. NiO hollow microspheres as efficient bifunctional electrocatalysts for Overall Water-Splitting. Int J Hydrogen Energy 2018;43:21665–74. https://doi.org/10.1016/j.ijhydene.2018.06.139.
[28] Jin S. Are metal chalcogenides, nitrides, and phosphides oxygen evolution catalysts or bifunctional catalysts? ACS Energy Lett 2017;2:1937–8. https://doi.org/10.1021/acsenergylett.7b00679.
[29] Finke CE, Omelchenko ST, Jasper JT, Lichterman MF, Read CG, Lewis NS, et al. Enhancing the activity of oxygen-evolution and chlorine-evolution electrocatalysts by atomic layer deposition of TiO_2. Energy Environ Sci 2019;12:358–65. https://doi.org/10.1039/C8EE02351D.
[30] Han JH, Lee SW, Kim SK, Han S, Hwang CS, Dussarrat C, et al. Growth of RuO_2 thin films by pulsed-chemical vapor deposition using RuO4 precursor and 5% H2 reduction gas. Chem Mater 2010;22:5700–6. https://doi.org/10.1021/cm101694g.
[31] Vante NA, Malakhov IV, Nikitenko SG, Savinova ER, Kochubey DI. The structure analysis of the active centers of Ru-containing electrocatalysts for the oxygen reduction. An in situ EXAFS study. Electrochim Acta 2002;47:3807–14. https://doi.org/10.1016/S0013-4686(02)00351-1.
[32] Kotz R, Lewerenz HJ, Stucki S. XPS studies of oxygen evolution on Ru and RuO_2 anodes. J Electrochem Soc 1983;130:825–9. https://doi.org/10.1149/1.2119829.
[33] Kelsey AS, Liang Q, Michael DB, Horn YS. Orientation-dependent oxygen evolution activities of rutile IrO_2 and RuO_2. J Phys Chem Lett 2014;5:1636–41. https://doi.org/10.1021/jz500610u.
[34] Jirkovsky J, Hoffmannova H, Klementova M, Krtil P. Particle size dependence of the electrocatalytic activity of nanocrystalline RuO_2 electrodes. J Electrochem Soc 2006;153:E111–8. https://doi.org/10.1149/1.2189953.
[35] Jirkovsky J, Klementova M, Krtil P. Particle size dependence of oxygen evolution reaction on nanocrystalline RuO_2 and $Ru_{0.8}Co_{0.2}O_{2-x}$. Electrochem Commun 2006;8:1417–22. https://doi.org/10.1016/j.elecom.2006.06.027.
[36] Lee YM, Suntivich J, May KJ, Perry EE, Horn YS. Synthesis and activities of rutile IrO_2 and RuO_2 nanoparticles for oxygen evolution in acid and alkaline solutions. J Phys Chem Lett 2012;3:399–404. https://doi.org/10.1021/jz2016507.
[37] Marques Mota F, Choi CH, Boppella R, Lee J-E, Kim DH. Arising synergetic and antagonistic effects in the design of Ni- and Ru-based water splitting electrocatalysts. J Mater Chem 2019;7:639–46. https://doi.org/10.1039/C8TA08535H.
[38] Reier T, Oezaslan M, Strasser P. Electrocatalytic oxygen evolution reaction (OER) on Ru, Ir, and Pt catalysts: a comparative study of nanoparticles and bulk materials. ACS Catal 2012;2:1765–72. https://doi.org/10.1021/cs3003098.
[39] Lyons MEG, Floquet S. Mechanism of oxygen reactions at porous oxide electrodes. Part 2—oxygen evolution at RuO_2, IrO_2 and $Ir_xRu_{1-x}O_2$ electrodes in aqueous acid and alkaline solution. Phys Chem Chem Phys 2011;13:5314–35.
[40] Lin Y, Tian Z, Zhang L, Ma J, Jiang Z, Deibert BJ, et al. Chromium-ruthenium oxide solid solution electrocatalyst for highly efficient oxygen evolution reaction in acidic media. Nat Commun 2019;10:162. https://doi.org/10.1038/s41467-018-08144-3.
[41] Shan J, Guo C, Zhu Y, Chen S, Song L, Jaroniec M, et al. Charge-redistribution-enhanced nanocrystalline Ru@IrOx electrocatalysts for oxygen evolution in acidic media. Chem 2019;5:445–59. https://doi.org/10.1016/j.chempr.2018.11.010.
[42] He R, Xu G, Wu Y, Shi K, Tang H, Ma P, et al. Nano-sized RuO_2 electrocatalyst improves the electrochemical performance for hydrogen oxidation reaction. Int J Hydrogen Energy 2019;44:5940–7. https://doi.org/10.1016/j.ijhydene.2019.01.114.
[43] Qiu T, Liang Z, Guo W, Gao S, Qu C, Tabassum H, et al. Highly exposed ruthenium-based electrocatalysts from bimetallic metal-organic frameworks for overall water splitting. Nano Energy 2019;58:1–10. https://doi.org/10.1016/j.nanoen.2018.12.085.
[44] Kunz V, Stepanenko V, Würthner F. Embedding of a ruthenium(II) water oxidation catalyst into nanofibers by self-assembly. Chem Commun 2015;51:290–3. https://doi.org/10.1039/C4CC08314H.
[45] Audichon T, Morisset S, Napporn TW, Kokoh KB, Comminges C, Morais C. Effect of adding CeO_2 to RuO_2–IrO_2 mixed nanocatalysts: activity towards the oxygen evolution

reaction and stability in acidic media. ChemElectroChem 2015;2:1128–37. https://doi.org/10.1002/celc.201500072.
[46] Puthiyapura VK, Pasupathi S, Basu S, Wua X, Su H, Varagunapandiyan N, Pollet B, Scott K. $Ru_xNb_{1-x}O_2$ catalyst for the oxygen evolution reaction in proton exchange membrane water electrolysers. Int J Hydrogen Energy 2013;38:8605–16. https://doi.org/10.1016/j.ijhydene.2013.04.100.
[47] Liang F, Yu Y, Zhou W, Xu X, Zhu Z. Highly defective CeO_2 as a promoter for efficient and stable water oxidation. J Mater Chem 2015;3:634–40. https://doi.org/10.1039/C4TA05770H.
[48] Demir E, Akbayrak S, Önal AM, Özkar S. Ceria supported ruthenium(0) nanoparticles: highly efficient catalysts in oxygen evolution reaction. J Colloid Interface Sci 2019;534:704–10. https://doi.org/10.1016/j.jcis.2018.09.075.
[49] Montini T, Melchionna M, Monai M, Fornasiero P. Fundamentals and catalytic applications of CeO_2-based materials. Chem Rev 2016;116:5987–6041. https://doi.org/10.1021/acs.chemrev.5b00603.
[50] Pahari SK, Pal P, Sinhamahapatra A, Saha A, Santra C, Ghosh SC, et al. Efficient oxidation of hydrocarbons over nanocrystalline $Ce_{1-x}Sm_xO_2$ (x= 0–0.1) synthesized using supercritical water. RSC Adv 2015;5:45144–51. https://doi.org/10.1039/c5ra05441a.
[51] Li P, Chen X, Li Y, Schwank JW. A review on oxygen storage capacity of CeO_2-based materials: influence factors, measurement techniques, and applications in reactions related to catalytic automotive emissions control. Catal Today 2019;327:90–115. https://doi.org/10.1016/j.cattod.2018.05.059.
[52] Pal P, Pahari SK, Sinhamahapatra A, Jayachandran M, Kiruthik GVM, Bajaj HC, et al. CeO_2 nanowires with high aspect ratio and excellent catalytic activity for selective oxidation of styrene by molecular oxygen. RSC Adv 2013;3:10837–47. https://doi.org/10.1039/c3ra23485a.
[53] Pal P, Singha RK, Saha A, Bal R, Panda AB. Defect-induced efficient partial oxidation of methane over nonstoichiometric Ni/CeO_2 nanocrystals. J Phys Chem C 2015;119:13610–8. https://doi.org/10.1021/acs.jpcc.5b01724.
[54] Sutradhar N, Sinhamahapatra A, Pahari S, Jayachandran M, Subramanian B, Bajaj HC, et al. Facile low-temperature synthesis of ceria and samarium-doped ceria nanoparticles and catalytic allylic oxidation of cyclohexene. J Phys Chem C 2011;115:7628–37. https://doi.org/10.1021/jp200645q.
[55] Satsuma A, Yanagihar M, Ohyam J, Shimizu K. Oxidation of CO over Ru/Ceria prepared by self-dispersion of Ru metal powder into nano-sized particle. Catal Today 2013;201:62–7. https://doi.org/10.1016/j.cattod.2012.03.048.
[56] Wang F, He S, Chen H, Wang B, Zheng L, Wei M, Evans DG, Duan X. Active site dependent reaction mechanism over Ru/CeO_2 catalyst toward CO_2 methanation. J Am Chem Soc 2016;138:6298–305. https://doi.org/10.1021/jacs.6b02762.
[57] Huang H, Dai Q, Wang X. Morphology effect of Ru/CeO_2 catalysts for the catalytic combustion ofchlorobenzene. Appl Catal B Environ 2014;158–159:96–105. https://doi.org/10.1016/j.apcatb.2014.01.062.
[58] Okal J, Zawadzki M, Kraszkiewicz P, Adamska K. Ru/CeO_2 catalysts for combustion of mixture of light hydrocarbons: effect of preparation method and metal salt precursors. Appl Catal Gen 2018;549:161–9. https://doi.org/10.1016/j.apcata.2017.09.036.
[59] Sutradhar N, Sinhamahapatra A, Pahari SK, Bajaj HC, Panda AB. Room temperature synthesis of protonated layered titanate sheets using peroxo titanium carbonate complex solution. Chem Commun 2011;47:7731–3. https://doi.org/10.1039/C1CC12116B.
[60] Giri AK, Pal P, Ananthakumar R, Jayachandran M, Mahanty S, Panda AB. 3D hierarchically assembled porous wrinkled-paper-like structure of $ZnCo_2O_4$ and Co-ZnO@ C as anode materials for lithium-ion batteries. Cryst Growth Des 2014;14:3352–9. https://doi.org/10.1021/cg500282n.
[61] Sinhamahapatra A, Pal P, Tarafdar A, Bajaj HC, Panda AB. Mesoporous borated zirconia: a solid acid–base bifunctional catalyst. ChemCatChem 2013;5:331–8. https://doi.org/10.1002/cctc.201200440.
[62] Shinagawa T, Garcia-Esparza AT, Takanabe K. Insight on Tafel slopes from a microkinetic analysis of aqueous electrocatalysis for energy conversion. Sci Rep 2015;5:13801. https://doi.org/10.1038/srep13801.